assumed a capacitance of 1 nF) and $\tau_\eta = 15$ ms. These were chosen so that for $S(t) = 0$, $A(\tau)$ and ISI histograms were similar to those observed under spontaneous conditions *in vivo*[20]. We set $N = 100$ to make local and global stimulation significantly distinct. The RAM stimulus variance was $W = 0.238\ \mathrm{nA}^2$, which resulted in firing statistics comparable to those of stimulated pyramidal neurons (Fig. 2). The feedback parameters were set to $g = 390\ \mathrm{S\,F^{-1}}$, $\alpha = 3$ ms, $V_r = V_{reset} = 0$ mV, to model the feedback as $GABA_A$ shunting inhibition, previously reported for interactions between bipolar and pyramidal cells[23]. The loop delay was set to $\tau_d = 12$ ms, allowing a fit to experimental data (Figs 1 and 2), and is also comparable to previously estimated values[22]. Equation (1) was integrated by a simple Euler–Maruyama[30] scheme with $\Delta t = 0.025$ ms. The effects of parameter heterogeneities were tested by choosing B_i and τ_m from gaussian distributions with mean values as given above. The results were qualitatively similar to the homogeneous case for distributions with coefficient of variations of 0.82 and 1.5 for the B_i and τ_m distributions, respectively.

Received 20 August; accepted 26 November 2002; doi:10.1038/nature01360.

1. Gray, C. & Singer, W. Stimulus-specific neuronal oscillations in orientation columns of cat visual cortex. *Proc. Natl Acad. Sci. USA* **86,** 1698–1702 (1989).
2. Sillito, A. M., Jones, H. E., Gerstein, G. L. & West, D. C. Feature-linked synchronization of thalamic relay cell firing induced by feedback from the visual cortex. *Nature* **369,** 479–482 (1994).
3. MacLeod, K. & Laurent, G. Distinct mechanisms for synchronization and temporal patterning of odor-encoding neural assemblies. *Science* **274,** 976–979 (1996).
4. Kashiwadani, H., Sasaki, Y. F., Uchida, N. & Kensaku, M. Synchronized oscillatory discharge of mitral/tufted cells with different molecular receptive ranges in the rabbit olfactory bulb. *J. Neurophysiol.* **82,** 1786–1792 (1999).
5. Stopfer, M., Bhagavan, S., Smith, B. H. & Laurent, G. Impaired odour discrimination on desynchronization of odour-encoding neural assemblies. *Nature* **390,** 70–74 (1997).
6. Friedrich, R. W. & Laurent, G. Dynamic optimization of odor representations by slow temporal patterning of mitral cell activity. *Science* **291,** 889–894 (2001).
7. Ahissar, E. & Vaadia, E. Oscillatory activity of single units in a somatosensory cortex of an awake monkey and their possible role in texture analysis. *Proc. Natl Acad. Sci. USA* **87,** 8935–8939 (1992).
8. Destexhe, A., Contreras, D. & Steriade, M. Mechanisms underlying the synchronization action of corticothalamic feedback through inhibition of thalamic relay cells. *J. Neurophysiol.* **79,** 999–1016 (1998).
9. Bressloff, P. C. & Coombes, S. Dynamics of strongly coupled spiking neurons. *Neural Comput.* **12,** 91–129 (2000).
10. Ernst, U., Pawelzik, K. & Geisel, T. Synchronization induced by temporal delays in pulse-coupled oscillators. *Phys. Rev. Lett.* **74,** 1570–1573 (1995).
11. Wang, X.-J. & Rinzel, J. Spindle rhythmicity in the reticularis thalami nucleus: synchronization among mutually inhibitory neurons. *Neuroscience* **53,** 899–904 (1993).
12. van Vreeswijk, C. & Hansel, D. Patterns of synchrony in neural networks with spike adaptation. *Neural Comput.* **13,** 959–992 (2001).
13. Paulis, Q., Baker, N. B. & Olivier, E. Emergent oscillations in a realistic network: the role of inhibition and the effect of the spatiotemporal distribution of input. *J. Comput. Neurosci.* **6,** 27–48 (1999).
14. Nelson, M. E. & MacIver, M. A. Prey capture in the weakly electric fish *Apteronotus leptorhynchus*: sensory acquisition strategies and electrosensory consequences. *J. Exp. Biol.* **202,** 1195–1203 (1999).
15. Metzner, W. Neural circuitry for communication and jamming avoidance in gymnotiform electric fish. *J. Exp. Biol.* **202,** 1365–1375 (1999).
16. Berman, N. J. & Maler, L. Neural architecture of the electrosensory lateral line lobe: adaptations for coincidence detection, a sensory searchlight and frequency-dependent adaptive filtering. *J. Exp. Biol.* **202,** 1243–1253 (1999).
17. Wessel, R., Koch, C. & Gabbiani, F. Coding of time-varying electric field amplitude modulations in a wave-type electric fish. *J. Neurophysiol.* **75,** 2280–2293 (1996).
18. Maler, L., Sas, E. K. & Rogers, J. The cytology of the posterior lateral line lobe of high frequency weakly electric fish (Gymnotoidei): differentiation and synaptic specificity in a simple cortex. *J. Comp. Neurol.* **195,** 87–139 (1981).
19. Dayan, P. & Abbott, L. F. *Theoretical Neuroscience* (MIT Press, Cambridge, Massachusetts, 2001).
20. Bastian, J. & Nguyenkim, J. Dendritic modulation of burst-like firing in sensory neurons. *J. Neurophysiol.* **85,** 10–22 (2001).
21. Maler, L. & Mugnaini, E. Correlating γ-aminobutyric acidergic circuits and sensory function in the electrosensory lateral line lobe of a gymnotiform fish. *J. Comp. Neurol.* **345,** 224–252 (1994).
22. Berman, N. J., Plant, J., Turner, R. & Maler, L. Excitatory amino acid transmission at a feedback pathway in the electrosensory system. *J. Neurophysiol.* **78,** 1869–1881 (1997).
23. Berman, N. J. & Maler, L. Interaction of $GABA_B$-mediated inhibition with voltage-gated currents of pyramidal cells: computational mechanism of a sensory searchlight. *J. Neurophysiol.* **80,** 3197–3213 (1998).
24. Glass, L. & Mackey, M. C. *From Clocks to Chaos* (Princeton Univ. Press, Princeton, New Jersey, 1988).
25. Doiron, B., Laing, C., Longtin, A. & Maler, L. Ghostbursting: a novel neuronal burst mechanism. *J. Comput. Neurosci.* **12,** 5–25 (2002).
26. Lemon, N. & Turner, R. W. Conditional spike backpropagation generates burst discharge in a sensory neuron. *J. Neurophysiol.* **84,** 1519–1530 (2000).
27. Bastian, J., Chacron, M. J. & Maler, L. Receptive field organization determines pyramidal cell stimulus encoding capability and spatial stimulus selectivity. *J. Neurosci.* **22,** 4577–4590 (2002).
28. Gabbiani, F., Metzner, W., Wessel, R. & Koch, C. From stimulus encoding to feature extraction in weakly electric fish. *Nature* **384,** 564–567 (1996).
29. Contreras, D., Destexhe, A., Sejnowski, T. J. & Steriade, M. Control of spatiotemporal coherence of a thalamic oscillation by corticothalamic feedback. *Science* **274,** 771–774 (1996).
30. Kloeden, P. E. & Platen, E. *Numerical Solutions to Stochastic Differential Equations* (Springer, Berlin, 1992).

Supplementary Information accompanies the paper on *Nature*'s website (http://www.nature.com/nature).

Acknowledgements We thank J. Lewis, C. Laing, R. W. Turner and M. Higley for reading the manuscript. Funding was provided by the National Science and Engineering Research Council (B.D., M.J.C., A.L.), the Canadian Institutes of Health Research (A.L., L.M.) and the National Institutes of Health (J.B.).

Competing interests statement The authors declare that they have no competing financial interests.

Correspondence and requests for materials should be addressed to B.D. (e-mail: bdoiron@science.uottawa.ca).

Fidelity in planar cell polarity signalling

Dali Ma*, Chung-hui Yang†, Helen McNeill‡, Michael A. Simon† & Jeffrey D. Axelrod*

* *Department of Pathology, Stanford University School of Medicine, Stanford, California 94305-5324, USA*
† *Department of Biological Sciences, Stanford University, Stanford, California 94305, USA*
‡ *Cancer Research UK, London Research Institute, 44 Lincoln's Inn Fields, London WC2A 3PX, UK*

The polarity of *Drosophila* wing hairs displays remarkable fidelity. Each of the approximately 30,000 wing epithelial cells constructs an actin-rich prehair that protrudes from its distal vertex and points distally. The distal location and orientation of the hairs is virtually error free, thus forming a nearly perfect parallel array. This process is controlled by the planar cell polarity signalling pathway[1–4]. Here we show that interaction between two tiers of the planar cell polarity signalling mechanism results in the observed high fidelity. The first tier, mediated by the cadherin Fat[5], dictates global orientation by transducing a directional signal to individual cells. The second tier, orchestrated by the 7-pass transmembrane receptor Frizzled[6,7], aligns each cell's polarity with that of its neighbours through the action of an intercellular feedback loop, enabling polarity to propagate from cell to cell[8]. We show that all cells need not respond correctly to the presumably subtle signal transmitted by Fat. Subsequent action of the Frizzled feedback loop is sufficient to align all the cells cooperatively. This economical system is therefore highly robust, and produces virtually error-free arrays.

A group of signalling molecules, including Frizzled (Fz)[7], Dishevelled (Dsh)[9], Flamingo (Fmi)[10,11], Van Gogh[12,13] and Prickle (Pk)[14] mediates planar cell polarity (PCP) signalling in various developing *Drosophila* tissues[1–4]. In wing cells, these proteins participate in an intercellular feedback loop that generates subcellular asymmetry and directs prehair location[8,15,16]. Frizzled on the distal side of one cell recruits Dsh to the membrane, thus stabilizing Fz localization, and simultaneously recruits Pk to the proximal side of the adjacent cell, where it prevents Dsh localization (Fig. 1a). A competition therefore occurs between Fz on either side of the intercellular boundary, amplifying small differences in Fz levels to all-or-none differences[8]. Coupled with the observation that cells do not accumulate high Fz levels and construct prehairs on two sides, this mechanism enables polarity to propagate from cell to cell (Fig. 1b). For example, removing Fz from a clone of cells produces a difference in Fz at the distal boundary of the clone that is reversed from the wild type, and this reversal propagates, resulting in the 'domineering non-autonomy' first described by ref. 6 (Fig. 1b). The question remains, however, of what initiates the imbalance of Fz activity along the proximal–distal axis of each cell in a wild-type wing. We have proposed previously that, in the eye, two

non-classical cadherins, Dachsous (Ds)[17] and Fat (Ft), and a type II transmembrane protein, Four-jointed (Fj)[18] work together to provide the Fz-dependent signal with directional cues[19]. In the imaginal eye disc, Ds and Fj, expressed in opposing gradients[19,20], function through Ft to enhance Fz activity in the R3 photoreceptor cell[21,22]. These proteins also affect PCP in the wing and abdomen[23–25]. We have investigated whether Fj, Ds and Ft provide global directional information in the wing.

Several observations suggest that the activities of Fj, Ds and Ft require Fz, and that they bias the orientation of Fz signalling in the wing, as they do in the eye[19]. Although *ft* mutant clones produce PCP phenotypes, Ft signalling requires Fz activity, as loss of *ft* function in large or small clones does not alter the characteristic polarity pattern of *fz* mutant wings (not shown). Fat localization (see below) is not affected in *fz, pk* and *fmi* mutant clones (not shown). Furthermore, in the absence of Fj, Ds or Ft, Dsh is membrane associated, and Dsh, Pk and Fmi remain asymmetrically localized (Fig. 1c, d, and data not shown), indicating that Fz continues to signal[15,16], although not always in the correct orientation. Similarly, double mutant combinations between *ds* and *fz* or *hs-fz* indicate that Fz functions, but abnormally, in *ds* mutants[23]. Therefore, in the wing, as in the eye[19], Fj, Ds and Ft orient the direction of the Fz-mediated intercellular feedback loop.

Four-jointed expression in the wing is graded, with the highest level at the distal margin (Fig. 1e; see also ref. 24). We found that

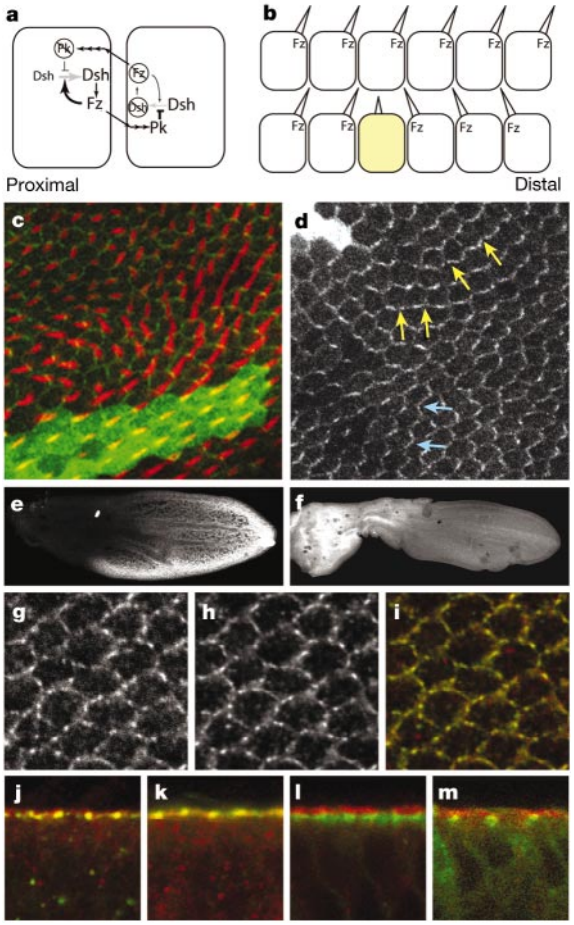

Figure 1 Four-jointed (Fj), Dachsous (Ds) and Fat (Ft) in the pupal wing. In all panels, distal is to the right. **a**, The Frizzled (Fz)-dependent intercellular feedback loop[8]. Circles with a slash through them indicate protein levels that are reduced or absent; bold arrows indicate dominant interactions. **b**, Diagram showing domineering non-autonomy[6]. The top row depicts wild-type wing cells with distal Fz, and prehairs pointing distally. In the bottom row, yellow represents a cell lacking Fz. In cells distal to the $fz^{-/-}$ cell, Fz localizes proximally and prehairs point proximally. **c**, $ft^{G\text{-}rv}$ clone, marked by the absence of green fluorescent protein (GFP), in a 33-h pupal wing. GFP clone marker and Dsh::GFP are stained green; prehairs visualized with phalloidin are red. **d**, $ft^{G\text{-}rv}$ mutant clone in a 30-h pupal wing showing GFP clone marker and Dsh::GFP. Dsh::GFP zig-zags inside the $ft^{G\text{-}rv}$ clone are misaligned in the anterior portion of this image (top; yellow arrows) compared to the posterior portions (blue arrows). **e**, **f**, Anti-βGal staining of *fj-lacZ* in a 24-h pupal wing (**e**), and Ds antibody staining in a 24-h pupal wing (**f**). **g**–**i**, Anti-Ft (**g**), anti-Ds (**h**) and an overlay (**i**: Ft, red; Ds, green) showing co-localization at cell boundaries in a 30-h pupal wing. **j**–**m**, Lateral view through edge cells showing co-localization of Ft (red) and Ds (green) (**j**), co-localization of Ft (red) and Discs lost (green), a marginal zone marker (**k**), Ft (red) apical to DE-cadherin::GFP (green; adherens junctions) (**l**), and Ft (red) apical to Fz::GFP (green) (**m**). Magnifications: **c**, **d**, ×700; **e**, ×12.5; **f**, ×10; **g**–**i**, ×1,400; **j**–**m**, ×700.

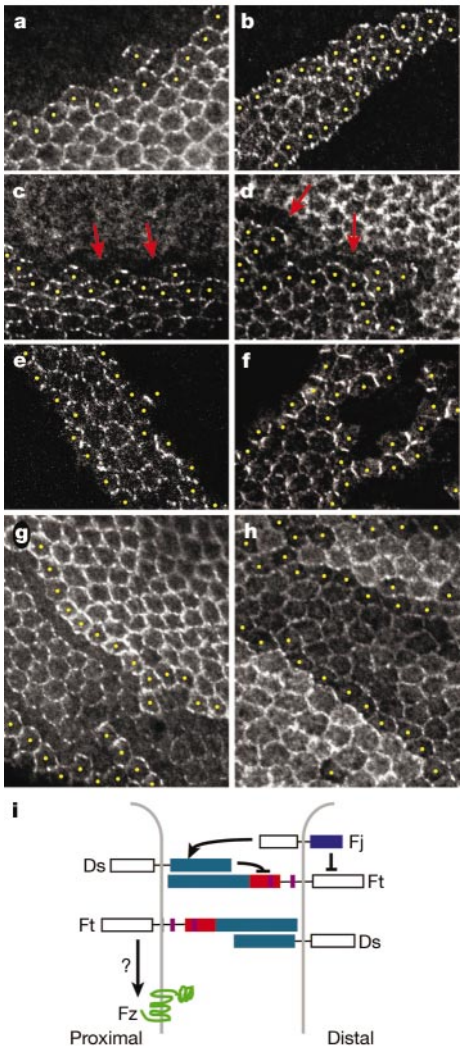

Figure 2 Dachsous and Ft protein localization, and dependence on Fj. **a**, **b**, Dachsous staining in a wing with ds^{UAO71} clones (**a**), and Ft staining in a wing with $ft^{G\text{-}rv}$ clones (**b**). Yellow dots mark the wild-type cells adjacent to the mutant clones in this and in the remaining panels. **c**, Dachsous staining in $ft^{G\text{-}rv}$ clones. **d**, Fat staining in ds^{UAO71} clones. Note the clone boundary effect in **c** and **d** (arrows). **e**, **f**, Dachsous (**e**) and Ft (**f**) staining in ds^{UAO71} $ft^{G\text{-}rv}$ double mutant clones. **g**, Dachsous staining is reduced inside a fj^{d1} clone. Note the boundary effect. **h**, Fat staining in a wing containing a fj^{d1} clone is elevated. **i**, Model illustrating a possible regulatory hierarchy among Fj, Ds and Ft. Straight arrows indicate activating interactions; blunt arrows indicate antagonistic activity. Fj at the proximal side of one cell may antagonize Ft directly or indirectly through promoting Ds in the neighbouring cell. Asymmetry in Fj and/or Ds may lead to asymmetric activity of Ft, which in turn facilitates Fz activity asymmetrically, by an unknown mechanism. Magnifications: **a**–**h**, ×700.

throughout pupal wing development, Ds expression is highest at the hinge, and lower distally (Fig. 1f, and data not shown). These patterns are reminiscent of Ds and Fj gradients in the eye disc, where Fj expression is highest at the equator and Ds expression is highest at the poles[19,20]. At higher resolution, Ds and Ft form punctate structures that localize together in a circumferential ring (Fig. 1g–i). However, unlike Fz and Dsh, there is no obvious asymmetry in Ds and Ft protein distribution[15,16]. In the apical–basal axis, Ds and Ft localize together with a marginal zone marker, and are apical to the adherens junctions, where Fz and Fmi are observed (Fig. 1j–m; see also refs 10, 16).

Staining in wings bearing mutant clones reveals that both Ds and Ft are present at the cell–cell boundary between wild-type and mutant tissues (Fig. 2a, b), suggesting that homotypic interactions are not required for their correct localization. This contrasts with Fmi, a cadherin needed for Fz localization[16], which requires homotypic interactions for maintenance of its own membrane localization[10]. Within a *ft* mutant clone, Ds becomes diffuse, suggesting that Ds localization depends on Ft (Fig. 2c). Furthermore, Ds staining is reduced in the *ft* mutant cells immediately abutting the wild-type cells, but appears stronger at the mutant–wild-type boundary than throughout the wild-type tissue. We interpret this 'clone-boundary effect' to indicate that Ds protein in the first row of mutant cells selectively localizes at boundaries in contact with cells expressing Ft. Similarly, Ft staining in *ds* mutant clones shows that Ft is distributed diffusely at the cell cortex, and protein levels appear elevated (Fig. 2d). A boundary effect is again seen, suggesting that Ft selectively localizes to boundaries in contact with Ds-expressing cells. These observations support a model in which the localization of Ds and Ft to punctate marginal zone structures requires intercellular heterotypic interactions. To test this, we examined Ds and Ft distribution at the boundaries between wild-type and *ds ft* double mutant clones, and found that, indeed, both proteins are lost from the membrane (Fig. 2e, f). Therefore, Ds and Ft maintain each other's wild-type localization in neighbouring cells.

Previous work in the eye indicated that Fj functions upstream of Ds, which is in turn upstream of Ft, and these interactions were

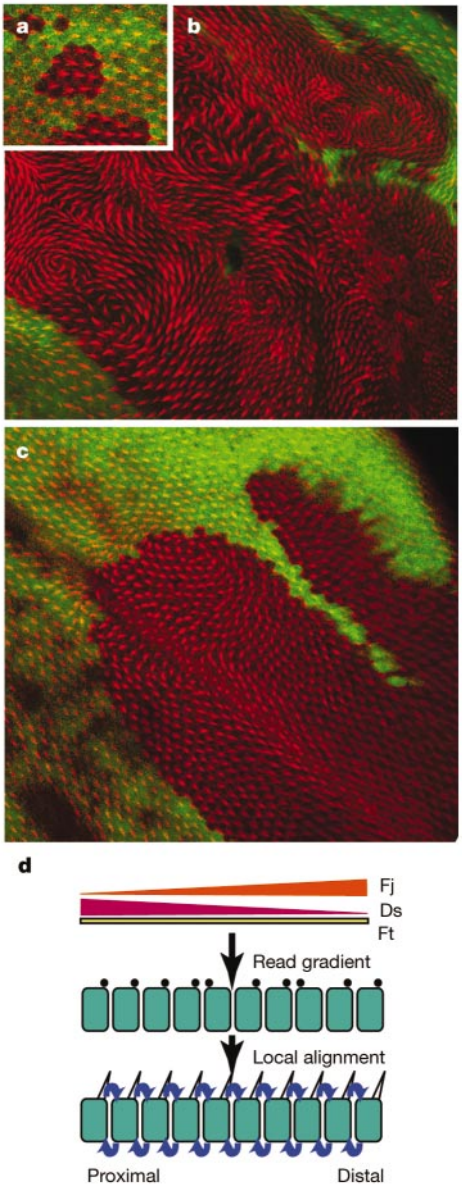

Figure 3 Fat clonal phenotypes indicate that global signalling interacts with the local alignment mechanism to achieve high fidelity. **a**, Small $ft^{l(2)fd}$ clones show no polarity disruption. **b**, **c**, Two large $ft^{l(2)fd}$ clones in which the prehairs form random swirls. Distal is bottom right. **d**, Model describing the interaction between the global signalling and local alignment mechanisms. Black dots indicate the tentative position each cell places its prehair after receiving gradient input from Ft. A fraction of cells may interpret the global input erroneously. Looped arrows represent the Fz-mediated feedback loop that aligns cells locally. This alignment mechanism corrects and compensates for the cells that have initially misinterpreted the gradient input. Magnifications: **a**, × 400; **b**, **c**, × 70.

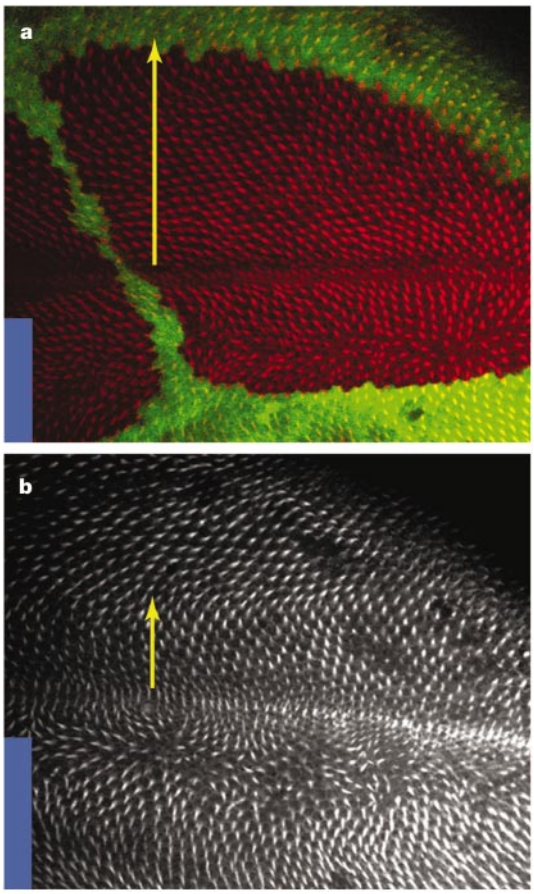

Figure 4 Loss of Ft in a large region enhances Fz domineering non-autonomy. **a**, A large $ft^{G\text{-}rv}$ clone overlapping the *decapentaplegic* (*dpp*) domain where Fz is overexpressed. **b**, A wing ectopically expressing Fz in the *dpp* region in a $ft^{G\text{-}rv}$ heterozygous background. The blue bars indicate the approximate extent of the *dpp* domain. Yellow arrows indicate the distance towards the anterior over which domineering non-autonomy extends. The distance is significantly greater in the $ft^{G\text{-}rv}$ clone (**a**) than in the control wing (**b**). Magnifications: **a**, **b**, × 80.

thought to be non-cell autonomous[19]. Consistent with this hierarchy, we found that Ds protein level is suppressed in *fj* wing clones (Fig. 2g). A boundary effect similar to that described above is seen, in which Ds preferentially associates with boundaries in contact with Fj-expressing cells. In contrast, Ft protein level is elevated in *fj* mutant clones (Fig. 2h). These observations support the proposal that Fj regulates Ds and Ft protein localization and activity. However, feedback regulation of *fj* expression by Ds and Ft, as seen in the eye[19], or reciprocal regulation of Fj protein localization by Ds and Ft have not been ruled out.

On the basis of these results, we propose that a series of intercellular interactions transmit directional information from Fj and Ds, through Ft, to the Fz-dependent feedback loop, as shown in Fig. 2i. The expression patterns of Fj and Ds may be the source of global directional information, although it is also possible that Fj and Ds transmit directional information from another source. Although the precise relationships between these proteins are not well defined, our data indicate that a heterotypic interaction between Ds and Ft is required to influence the direction of Fz signalling.

We examined more closely the consequences of disabling this global directional signal to test the prediction that in its absence, local Fz-mediated alignment would occur, but that it would be uncoupled from the global axes of the wing. We therefore examined the phenotypes of *ft* or *ds ft* double mutant clones. These genotypes produced essentially identical results (not shown). Very large *ft* mutant clones often show marked swirls (Fig. 3b, c). Unlike *fz*, *ds*, or *fj* mutants[23,24,26], we observed no reproducible pattern in a given region from one wing to another. Furthermore, in these large clones, the cell–cell alignment shows continuity within and across the clone boundaries, consistent with the observation that Fz signalling is intact. In contrast, in small *ft* mutant clones, the orientation of prehairs is always normal (Fig. 3a). This observation suggests the possibility that correct polarity within these small *ft* mutant clones is maintained by the intact function of the Fz-dependent feedback loop and its ability to propagate polarity. Within large *ft* clones, local alignment persists, consistent with Fz function, but the direction of this polarity signalling becomes abnormal, indicating that Fz-mediated polarity propagation cannot proceed in the correct direction over large distances in the absence of the global directional signal. We therefore propose that in the wild type, cells respond to a global directional cue mediated by Ft, but all cells may not respond accurately (Fig. 3d). Indeed, the cue is predicted to be subtle. The subsequent action of the Fz feedback loop to produce local alignment is proposed to correct errors in the initial reading of the global cue, resulting in a high-fidelity response.

Experimentally induced boundaries between cells expressing high and low Fz cause polarity to propagate in an abnormal direction through wild-type tissue. Our model predicts that this propagation will be constrained by the global directional cue mediated by Ft. For example, distal to *fz* clones, polarity is reversed in a limited domain[6]; the extent of the abnormal polarity may be limited by the global Ft-dependent signal. To test this hypothesis, we induced domineering non-autonomy by overexpressing Fz in the *decapentaplegic* (*dpp*) domain, a proximal–distal stripe between veins L3 and L4. This results in abnormal PCP both within the *dpp* domain, and at a distance anterior to the *dpp* domain, where the prehairs point away from the *fz*-overexpressing cells (Fig. 4b; refs 10, 27). We then eliminated the global cue by removing *ft* in large clones that span this region, and found that the extent of domineering non-autonomy is increased, spanning the length of the clone (Fig. 4a). It has also been observed that *fz* mutant clones show enhanced domineering non-autonomy when the global signal is partially disabled in *ds* mutant wings[23]. These results are consistent with our hypothesis that the Ft-mediated signal provides a directional cue that orients the action of the Fz-dependent alignment mechanism.

We have presented a model in which the interaction between the global directional signal, mediated by Ft, and a local Fz-dependent cell–cell alignment mechanism is important for achieving a high-fidelity PCP response. This interaction results in a highly robust mechanism requiring a minimum amount of complexity. How much, if any, directional information is encoded in the expression patterns of Fj and Ds, or whether they transduce information from other sources, remains to be determined. Indeed, we observe that the ability of Fj to regulate Ds and Ft localization is strongly biased towards the posterior of the wing, suggesting that an as yet unidentified component may have this function in the anterior. It will also be important to determine how Ft influences the orientation of the Fz local alignment mechanism. Our model establishes a framework for understanding the interaction between the global and local PCP signals, and how that interaction produces a high-fidelity response. □

Methods

Genetics

We used the following fly strains: $ft^{G\text{-}rv}$ (ref. 5), $ft^{l(2)fd}$ (ref. 28), ds^{UAO71} *FRT40A* (ref. 23), *FRT42D* fj^{N7} (*fj-lacZ*; ref. 29), *FRT42D* fj^{d1} (ref. 24), *dsh::GFP* (ref. 15), *UASFz* (ref. 27), *dpp–Gal4* (Bloomington), DE-cadherin::GFP, *Fz::GFP* (ref. 16), fz^{R52} and fz^{D21} (P. Adler).

Mutant clones in the pupal wings were generated by FRT-FLP-mediated mitotic recombination[30]. Clones were marked with ubiquitously expressed green fluorescent protein (ubGFP). T155 stocks were a gift from J. Duffy. The genotypes for the experiments are: $ft^{G\text{-}rv}$ *FRT40A/UbGFP FRT40A; dsh::GFP/T155Gal4 UASflp*, $ft^{l(2)fd}$ *FRT40A/UbGFP FRT40A; dsh::GFP/T155Gal4 UASflp*, ds^{UAO71} *FRT40A/UbGFP FRT40A; dsh::GFP/T155Gal4 UASflp*, *FRT42D* fj^{N7}*/FRT42D UbGFP; dsh::GFP/T155Gal4 UASflp*, *FRT42D* fj^{d1}*/FRT42D UbGFP; T155Gal4 UASflp* and *hsflp;* $ft^{G\text{-}rv}$ *FRT40A/UbGFP FRT40A; UASFz/dppGal4*.

All flies were reared at 23–25 °C. Heat-shock clones were induced at 37 °C for 45 min. White pre-pupae were collected and allowed to age at 25 °C. All clones were induced during third instar, before PCP signalling. No perdurance of Ft or Ds was detected by immunofluorescence in clones of any size.

Immunofluorescence

Rat anti-Ft[19] and anti-Ds[19] (all except Fig. 1g–i) were used at 1:100. Rabbit anti-Ds (Fig. 1g, h), raised against THLPHVSLPRHGHAPQPRGNVGTRM from the cytoplasmic domain, was used at 1:500. Their specificity is demonstrated by lack of staining in clones of the corresponding mutant cells (Fig. 2a, b; and data not shown). Mouse anti-βGal (Promega) was used at 1:200. Rabbit anti-Discs lost (M. Bhat and H. Bellen) was used at 1:500. Secondary Alexa488- and Alexa594-conjugated anti-rat and anti-rabbit antibodies and Alexa568-conjugated phalloidin were from Molecular Probes. Pupal wings were dissected and stained as described in ref. 15, and visualized with a Nikon laser scanning confocal microscope.

Received 27 August; accepted 12 December 2002; doi:10.1038/nature01366.
Published online 19 January 2003.

1. Shulman, J. M., Perrimon, N. & Axelrod, J. D. Frizzled signaling and the developmental control of cell polarity. *Trends Genet.* **14,** 452–458 (1998).
2. Adler, P. N. Planar signaling and morphogenesis in *Drosophila*. *Dev. Cell* **2,** 525–535 (2002).
3. Strutt, D. I. The asymmetric subcellular localisation of components of the planar polarity pathway. *Semin. Cell Dev. Biol.* **13,** 225–231 (2002).
4. Tree, D. R. P., Ma, D. & Axelrod, J. D. A three-tiered mechanism for regulation of planar cell polarity. *Semin. Cell Dev. Biol.* **13,** 217–224 (2002).
5. Mahoney, P. A. *et al.* The fat tumour suppressor gene in *Drosophila* encodes a novel member of the cadherin gene superfamily. *Cell* **67,** 853–868 (1991).
6. Vinson, C. R. & Adler, P. N. Directional non-cell autonomy and the transmission of polarity information by the *frizzled* gene of *Drosophila*. *Nature* **329,** 549–551 (1987).
7. Vinson, C. R., Conover, S. & Adler, P. N. A *Drosophila* tissue polarity locus encodes a protein containing seven potential transmembrane domains. *Nature* **338,** 263–264 (1989).
8. Tree, D. R. P. *et al.* Prickle mediates feedback amplification to generate asymmetric planar cell polarity signaling. *Cell* **109,** 371–381 (2002).
9. Klingensmith, J., Nusse, R. & Perrimon, N. The *Drosophila* segment polarity gene dishevelled encodes a novel protein required for response to the wingless signal. *Genes Dev.* **8,** 118–130 (1994).
10. Usui, T. *et al.* Flamingo, a seven-pass transmembrane cadherin, regulates planar cell polarity under the control of Frizzled. *Cell* **98,** 585–595 (1999).
11. Chae, J. *et al.* The *Drosophila* tissue polarity gene starry night encodes a member of the protocadherin family. *Development* **126,** 5421–5429 (1999).
12. Taylor, J., Abramova, N., Charlton, J. & Adler, P. N. Van gogh. A new *Drosophila* tissue polarity gene. *Genetics* **150,** 199–210 (1998).
13. Wolff, T. & Rubin, G. M. Strabismus, a novel gene that regulates tissue polarity and cell fate decisions in *Drosophila*. *Development* **125,** 1149–1159 (1998).
14. Gubb, D. *et al.* The balance between isoforms of the prickle LIM domain protein is critical for planar polarity in *Drosophila* imaginal discs. *Genes Dev.* **13,** 2315–2327 (1999).
15. Axelrod, J. D. Unipolar membrane association of Dishevelled mediates Frizzled planar cell polarity signaling. *Genes Dev.* **15,** 1182–1187 (2001).
16. Strutt, D. I. Asymmetric localization of Frizzled and the establishment of cell polarity in the *Drosophila* wing. *Mol. Cell* **7,** 367–375 (2001).

17. Clark, H. F. *et al.* Dachsous encodes a member of the cadherin superfamily that controls imaginal disc morphogenesis in *Drosophila*. *Development* **9,** 1530–1542 (1995).
18. Villano, J. L. & Katz, F. N. four-jointed is required for intermediate growth in the proximal-distal axis in *Drosophila*. *Development* **121,** 2767–2777 (1995).
19. Yang, C., Axelrod, J. D. & Simon, M. A. Regulation of Frizzled by Fat-like cadherins during planar polarity signaling in the *Drosophila* compound eye. *Cell* **108,** 675–688 (2002).
20. Zeidler, M. P., Perrimon, N. & Strutt, D. I. The four-jointed gene is required in the *Drosophila* eye for ommatidial polarity specification. *Curr. Biol.* **9,** 1363–1372 (1999).
21. Fanto, M. & Mlodzik, M. Asymmetric Notch activation specifies photoreceptors R3 and R4 and planar polarity in the *Drosophila* eye. *Nature* **397,** 523–526 (1999).
22. Cooper, M. T. & Bray, S. J. Frizzled regulation of Notch signalling polarizes cell fate in the *Drosophila* eye. *Nature* **397,** 526–530 (1999).
23. Adler, P. N., Charlton, J. & Liu, J. Mutations in the cadherin superfamily member gene dachsous cause a tissue polarity phenotype by altering frizzled signaling. *Development* **125,** 959–968 (1998).
24. Zeidler, M. P., Perrimon, N. & Strutt, D. I. Multiple roles for four-jointed in planar polarity and limb patterning. *Dev. Biol.* **228,** 181–196 (2000).
25. Casal, J., Struhl, G. & Lawrence, P. Developmental compartments and planar polarity in *Drosophila*. *Curr. Biol.* **12,** 1189–1198 (2002).
26. Gubb, D. & Garcia-Bellido, A. A genetic analysis of the determination of cuticular polarity during development in *Drosophila melanogaster*. *J. Embryol. Exp. Morphol.* **68,** 37–57 (1982).
27. Adler, P. N., Krasnow, R. E. & Liu, J. Tissue polarity points from cells that have higher Frizzled levels towards cells that have lower Frizzled levels. *Curr. Biol.* **7,** 940–949 (1997).
28. Bryant, P. J., Huettner, B., Held, L. I. Jr, Ryerse, J. & Szidonya, J. Mutations at the fat locus interfere with cell proliferation control and epithelial morphogenesis in *Drosophila*. *Dev. Biol.* **129,** 541–554 (1988).
29. Buckles, G. R., Rauskolb, C., Villano, J. L. & Katz, F. N. Four-jointed interacts with dachs, abelson and enabled and feeds back onto the Notch pathway to affect growth and segmentation in the *Drosophila* leg. *Development* **128,** 3533–3542 (2001).
30. Xu, T. & Rubin, G. M. Analysis of genetic mosaics in developing and adult *Drosophila* tissues. *Development* **117,** 1223–1237 (1993).

Acknowledgements We thank D. Bilder for advice, J. Duffy and the Bloomington stock center for fly strains, and members of the Axelrod laboratory for discussions of the work and comments on the manuscript. This work was supported by the NIH (J.D.A.).

Competing interests statement The authors declare that they have no competing financial interests.

Correspondence and requests for materials should be addressed to J.D.A. (e-mail: jaxelrod@stanford.edu).

Haematopoietic stem cells retain long-term repopulating activity and multipotency in the absence of stem-cell leukaemia SCL/*tal-1* gene

Hanna K. A. Mikkola, Jenny Klintman, Haidi Yang, Hanno Hock, Thorsten M. Schlaeger, Yuko Fujiwara & Stuart H. Orkin

Department of Pediatric Oncology, Children's Hospital and the Dana Farber Cancer Institute, Harvard Medical School and Howard Hughes Medical Institute, Boston, Massachusetts 02115, USA

The production of blood cells is sustained throughout the lifetime of an individual by haematopoietic stem cells (HSCs)[1]. Specification of HSCs from mesoderm during embryonic development requires the stem cell leukaemia *SCL/tal-1* gene product[2–6]. Forced expression of *SCL/tal-1* strongly induces blood formation in embryos, indicating that this gene has a dominant role in commitment to haematopoiesis[7,8]. In the adult haematopoietic system, expression of *SCL/tal-1* is enriched in HSCs and multipotent progenitors, and in erythroid and megakaryocytic lineages[9–11], consistent with roles for this factor in adult haematopoiesis. Here we assess by conditional gene targeting whether *SCL/tal-1* is required continuously for the identity and function of HSCs. We find that *SCL/tal-1* is dispensable for HSC engraftment, self-renewal and differentiation into myeloid and lymphoid lineages; however, the proper differentiation of erythroid and megakaryocytic precursors is dependent on *SCL/tal-1*. Thus, *SCL/tal-1* is essential for the genesis of HSCs, but its continued expression is not essential for HSC functions. These findings contrast with lineage choice mechanisms, in which the identity of haematopoietic lineages requires continuous transcription factor expression[12,13].

Knockout of the *SCL/tal-1* gene is embryonic lethal in mice owing to a complete failure of haematopoiesis[2,5], thereby precluding a simple study of the requirement for this gene in bone marrow (BM) haematopoiesis in adults. We therefore constructed a conditional mutant[14] *SCL/tal-1* strain ($SCL^{fl/fl}$; Fig. 1a). Germline Cre-recombinase-mediated deletion of the *loxP*-flanked (floxed) basic helix–loop–helix (bHLH) region of the gene recapitulated the phenotype of the conventional knockout, as anticipated (data not shown). To inactivate the *SCL/tal-1* gene in the adult haematopoietic compartment, we bred the $SCL^{fl/fl}$ strain with MxCre mice in which Cre is expressed after the induction of interferon by administration of poly(I)-poly(C) (pIpC)[15].

Whereas partial Cre-mediated deletion occurred in many tissues, excision in haematopoietic cells, including HSCs, was efficient after seven injections of pIpC administered every other day (data not shown). Peripheral blood counts were not changed significantly in pIpC-treated heterozygous ($SCL^{fl/wt}$) mice (data not shown). In pIpC-treated $SCL^{fl/fl}$ mice, but not in control $SCL^{fl/wt}$ mice, excision of *SCL/tal-1* resulted in moderate anaemia and thrombocytopenia, with nadirs at 4 and 2 weeks after the initiation of pIpC treatment, respectively, and in about 5% lethality (data not shown). The floxed allele was excised completely in haematopoietic cells of pIpC-treated $SCL^{fl/wt}$ mice, as assessed by three-primer, genomic polymerase chain reaction (PCR) of the DNA from peripheral blood cells and individual colonies grown from BM cells (Fig. 1b and data not shown). In surviving pIpC-treated $SCL^{fl/fl}$ mice, however, an intact floxed allele was detected by PCR in a fraction of peripheral blood and BM cells (Fig. 1b and data not shown). These data indicate that *SCL/tal-1* may be required, as thought previously, for

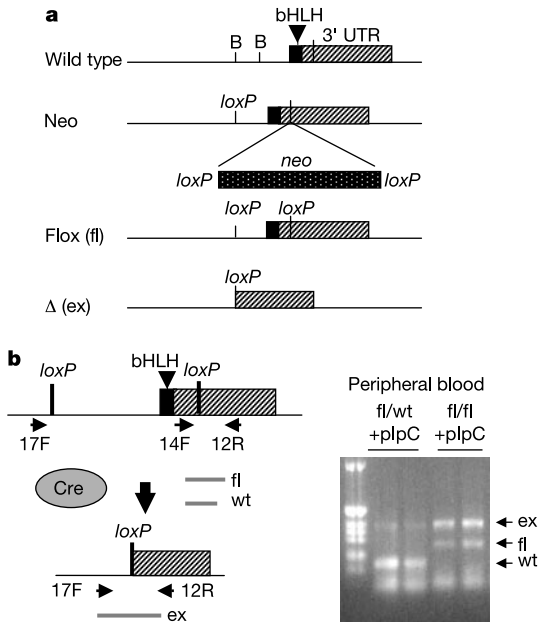

Figure 1 Inducible inactivation of the *SCL/tal-1* locus *in vivo*. **a**, Conditional targeting of the *SCL/tal-1* locus. The floxed *neomycin* cassette was introduced at a unique *Xba*I site in the 3′ untranslated region (3′ UTR). B, *Bam*HI site. **b**, Deletion of the floxed region was monitored by semiquantitative, three-primer PCR. Peripheral blood PCR from two representative examples at 12 weeks after pIpC administration is shown on the right. ex, excised; fl, floxed; wt, wild-type products.